# Engineering the acidity and accessibility of the zeolite ZSM-5 for efficient bio-oil upgrading in catalytic pyrolysis of lignocellulose

Héctor Hernando,*[a] Ana M. Hernández-Giménez,[b] Cristina Ochoa-Hernández,[c,†] Pieter C. A. Bruijnincx,[b] Klaartje Houben,[d] Marc Baldus,[d] Patricia Pizarro,[a,e] Juan M. Coronado,[a] Javier Fermoso,[a] Jiří Čejka,[c] Bert M. Weckhuysen,[b] David P. Serrano[a,e]*

[a.] *Thermochemical Processes Unit, IMDEA Energy Institute, 28935, Móstoles, Madrid, Spain*
[b.] *Inorganic Chemistry and Catalysis, Debye Institute for Nanomaterials Science, Utrecht University, Universiteitsweg 99, 3584 CG Utrecht, The Netherlands*
[c.] *J. Heyrovský Institute of Physical Chemistry, Academy of Sciences of the Czech Republic, v.v.i., 182 23, Prague 8, Czech Republic*
[d.] *NMR Spectroscopy, Bijvoet Center for Biomolecular Research, Department of Chemistry, Utrecht University, Padualaan 8, 3584 CH Utrecht, The Netherlands*
[e.] *Chemical and Environmental Engineering Group, ESCET, Rey Juan Carlos University, 28933, Móstoles, Madrid, Spain*
*† Current affiliation address: Department of Heterogeneous Catalysis, Max-Planck-Institut für Kohlenforschung, 45470, Mülheim an der Ruhr, Germany*

## Supporting information

## Experimental

### Catalyst preparation

**Zeolite samples.** Two ZSM-5 zeolites were selected as catalytic supports: a nanocrystalline ZSM-5 provided by CLARIANT (HCZP 90) denoted as n-ZSM-5; and a microcrystalline material (1-4 μm) synthesized by SILKEM, which was subjected to desilication by treatment with a 1.4 M NaOH solution at 65 °C for 30 min (solution/zeolite mass ratio = 5) to generate mesopores, being denoted as h-ZSM-5. After desilication, the sample was ion-exchanged with an ammonium sulphate solution and calcined in air at 550 °C to obtain the acid form.

**$ZrO_2$ incorporation.** $ZrO_2$ was introduced in both h-ZSM-5 and n-ZSM-5 in a proportion of 10 wt% by wet impregnation in two steps and using ethanol as solvent, followed by calcination in static air. Initially, 50% of the total metal precursor required (zirconium (IV) acetylacetonate, Aldrich, 97%) was dissolved in ethanol (10 $ml \cdot g_{support}^{-1}$) and contacted with the support. The mixture was kept stirring for 6 h at 40 °C and the solvent was then removed using a rotary evaporator. After that, the sample was dried at 100 °C in an oven overnight. Using this same procedure, the second half of the zirconium precursor solution was added to the support. Finally, the sample was calcined at 450 °C for 6 h to obtain the final $ZrO_2$/h-ZSM-5 and $ZrO_2$/n-ZSM-5 samples.

### Catalyst characterisation

**X-ray diffraction.** X-ray diffraction (XRD) patterns of the parent ZSM-5 zeolites and $ZrO_2$ supported catalysts were recorded with a Philips PW 3040/00 X'Pert MPD/MRD diffractometer using Cu Kα radiation (λ = 1.542 Å), operated at 45 kV and 40 mA.

**Electronic microscopy - energy dispersive X-ray analysis.** The samples were analysed by Transmission Electronic Microscopy (TEM) using a Philips TECNAI 20 instrument operating at 200 kV. Likewise, Scanning Electron Microscopy (SEM) images and energy dispersive X-ray spectroscopy (EDX) were recorded using a FEI XL30SFEG microscope. The samples were sprinkled on an aluminium stub with a carbon sticker. Pt sputter coating was avoided to prevent overlap of the Pt and Zr signals in the EDX measurements. Quantification of Zr average has been based counting on Si, Al, O and Zr elements. SEM images were recorded in secondary electron (SE) mode.

**Ar adsorption-desorption isotherms.** The textural properties of the assayed catalysts were determined by argon adsorption–desorption isotherms at −186 °C in an AUTOSORB iQ Analyzer System from Quantachrome Instruments. The samples were previously degassed at 300 °C under vacuum for 3 h. The total surface area was determined applying the Brunauer–Emmett–Teller (BET) equation. The pore size distribution and the contribution of micro- and mesopores to the textural properties were calculated using the adsorption branch of the isotherms by means of the NL-DFT (Non Local Density Functional Theory) model assuming cylindrical pore geometry.

**Inductively coupled plasma-optical emission spectroscopy.** The aluminium and zirconia contents of the zeolite samples were measured by inductively coupled plasma-optical emission spectroscopy (ICP-OES) using a Perkin Elmer Optima 7300AD instrument. Thereby, the samples were digested in a mixture of HF and $HNO_3$ in a microwave oven (Anton Paar MW3000).

**Acidity measurements.** The Brønsted and Lewis acid sites (BAS and LAS, respectively) were quantified by pyridine adsorption, followed by FTIR spectroscopy. Self-supporting wafers (ca. 10 $mg/cm^2$) were prepared and activated at 450 °C for 4 h under vacuum. Subsequently, 3 torr of pyridine were introduced into the system and the adsorption took place at 150 °C for 20 min. The strength of BAS and LAS was determined at different evacuation temperatures (150, 250, 350 and 450 °C). Thereby, after 20 min of desorption at high vacuum, spectra were recorded at room temperature with a 4 $cm^{-1}$ resolution in the 4000-400 $cm^{-1}$ range by means of a Nicolet FTIR spectrometer equipped with a MCT detector. The concentration of BAS ($C_B$) and LAS ($C_L$) was calculated using specific FTIR bands and the corresponding molar extinction coefficients, as explained elsewhere [1,2].

**Raman spectroscopy.** Raman spectroscopy was performed with a Renishaw InVia microscope, using 785 nm laser excitation, through

a 20x long working distance objective. Spectra were acquired using a 100% laser excitation power, for 5 accumulations at a 20 s exposure. In the case of the monoclinic $ZrO_2$ powder used as reference (Aldrich, nanopowder, <100 nm), the parameters were the same as for the catalyst powders except for 50% laser excitation power.

**Magic angle spinning solid-state nuclear magnetic resonance.** $^{27}Al$ magic angle spinning solid-state nuclear magnetic resonance (MAS ssNMR) experiments were performed at 11.7 T (n-ZSM-5) and 9.4 T (h-ZSM-5) (500 and 400 MHz $^{1}H$ Larmor frequency) on a Bruker Avance III spectrometer equipped with a 3.2 mm MAS probe. Spectra were recorded at ambient temperature using 18 kHz MAS, for the h-ZSM-5 catalyst, and 15 kHz MAS for the n-ZSM-5 zeolite. RF fields of 50 kHz and 40 kHz were respectively used for the $^{27}Al$ π/12 pulse followed by 26 ms acquisition. 10240 scans were accumulated using an inter-scan delay of 1 s. The $^{27}Al$ chemical shift was externally referenced to an aqueous aluminium nitrate solution. The 1D spectra were processed using a line-broadening of 100 Hz.

A zero-quantum (ZQ) filtered multiple-quantum magic angle spinning (MQ-MAS) pulse- sequence was used to correlate the $^{27}Al$ isotropic chemical shift (F1) with the quadrupolar line-shape (F2) [3]. The excitation and conversion pulses were applied with an RF field of 62 kHz. For the selective pulse following the Z-filter delay an RF field of 6.5 kHz was used. The incrementation time for the indirect dimension was set to one rotation period and 36 increments were recorded. The direct acquisition time was set to 2.5 ms and 696 scans were accumulated using an inter-scan delay of 2 s. MQ-MAS data were Fourier transformed and sheared, using the software of Bruker Topspin3.5, and 250 Hz line-broadening was applied in both dimensions.

The 1D NMR spectra were deconvoluted using a Gaussian multipeak fitting function in the Origin 9.1 software. The areas under the curves were fitted based on the Levenberg-Marquardt least-squares algorithm to generate fits from starting peak positions observed in the corresponding MQ MAS NMR spectra. The areas under the peaks were used to estimate the ratio between framework and extra-framework Al species.

**UV-Vis micro-spectroscopy.** UV-Vis micro-spectroscopy was performed in an in-situ cell (FTIR600, Linkam Scientific Instruments) equipped with a temperature controller (Linkam TMS 93). The microscopy set-up used is based on an Olympus BX41 upright microscope with a 50 x 0.5 NA-high (NA: numerical aperture) working distance microscope objective. A 75 W tungsten lamp was used for illumination. The microscope was equipped with a 50/50 double-viewport tube, which accommodated a CCD video camera (ColorView IIIu, Soft Imaging System GmbH) and an optical fibre mount. A 200 mm-core fibre connected the microscope to a CCD UV/Vis spectrometer (AvaSpec-2048TEC, Avantes).

Selective catalyst staining by 4-fluorostyrene oligomerization was followed in-situ by UV-Vis micro-spectroscopy. After preheating the catalysts at 100 °C for 10 min, 15 µl of 4-fluorostyrene was added per 10 mg of sample. The first in-situ spectra of the stained powder catalyst were recorded 5 min after addition for 15 min.

**Confocal fluorescence microscopy.** Confocal fluorescence microscopy (CFM) images of the stained materials were acquired using a Nikon Eclipse 90i confocal microscope with a 100 x 0.73 NA dry objective. Excitation light was provided by focusing three specific laser lines, 488, 561 and 642 nm, simultaneously on the desired sample, located in an open cell (Linkam Instruments, FTIR 600). The microscope was equipped with a Nikon A1 scan head, accommodating the optics, which couple fibre optics for excitation and emission light microscope. A spectral analyser in the Nikon A1 system was equipped with 32 photomultiplier tubes (PMTs) set to collect emission light in the region of ca. 450–700 nm, with a resolution of 6 nm. Following the same procedure as for in-situ UV-Vis micro-spectroscopy, 4-fluorostyrene oligomerization staining was also followed in-situ by CFM. In addition, ex-situ fluorescence spectra were recorded on the samples 30 min after the reaction.

**Biomass feedstock**

The lignocellulosic biomass employed in this study was acid-washed wheat straw (WS-ac), obtained from agricultural residues of Segovia province (Spain). The raw biomass was ground into a particle size of 0.5-1 mm and then subjected to a de-ashing treatment by acid washing. Thereby, a representative amount of biomass was dispersed into a 1 wt% $HNO_3$ solution (20 $ml_{dis} \cdot g^{-1}_{biomass}$) at 50 °C for 2 h. The sample was then filtered, washed with Milli-Q water till neutral pH and finally dried at 105 °C for 2 days. This pre-treatment was applied to minimize the interferences of the intrinsic catalytic effects of the mineral matter present in the raw biomass.

**Biomass pyrolysis tests**

The details of the lab-scale experimental setup here used for the catalytic fast-pyrolysis tests have been provided elsewhere [4]. The reaction system consists of a downdraft fixed bed reactor with two differentiated zones physically separated, one for the primary thermal pyrolysis and other for the vapour catalytic upgrading, heated and controlled by two independent electric furnaces and K thermocouples, respectively. All the experiments were carried out using 4 g of *WS-ac* sample. For the catalytic experiments, 1.6 and 2.8 g (0.4 and 0.7 g/g catalyst/biomass ratio, respectively) were loaded. Catalysts were pelletized into particles with a size between 0.180 – 0.250 µm to avoid an excessive pressure drop and to ease their recovery after reaction. The pyrolysis tests were carried out at atmospheric pressure and temperatures of 550 and 400 °C for the pyrolysis and catalytic zones, respectively, using 100 $cm^3 \cdot min^{-1}$ of $N_2$ as carrier gas.

Once the levels of $O_2$ were dropped down to < 0.1 vol% in the reaction system and the selected temperatures were reached, the biomass feeding valve was opened and the biomass was introduced into the reactor. Consequently, the pyrolysis reaction occurred and char (carbonaceous solid by-product) and pyrolysis vapours were formed. The solid fraction was accumulated in the thermal zone, while vapours and permanent gases were swept by the $N_2$ flow and passed through the catalyst bed. The vapours leaving the reactor were condensed by a series of 125 $cm^3$ flasks refrigerated by an ice-

water bath kept at 0 °C. The non-condensable gases were passed to a sampling bag placed at the end of the line.

The different fractions formed in the pyrolysis process (bio-oil, char, coke and non-condensable gases) were collected, quantified and subjected to detailed compositional analysis, as next described. The bio-oil fraction expressed on a water-free basis is denoted as bio-oil*.

**Characterization of the products obtained in the biomass pyrolysis tests.**

Proximate analyses of the biomass were performed following European standards, including moisture (UNE-EN 14774-1:2010), ash (UNE-EN 14775:2010), and volatile matter (UNE-EN 15148:2010) contents. The moisture content was determined by weight difference of a representative amount of biomass sample after being dried in an oven at 105 °C for 3 h. The ash content present was calculated by combusting a representative amount of biomass (20 g, previously dried) at 815 ºC with 100 $cm^3 \cdot min^{-1}$ air flow for 2 h. The chemical composition of the ash was measured by ICP-OES. Volatile matter of biomass and char was determined by thermogravimetric analysis (TGA) using a NETZSCH STA 449 thermobalance from the weight loss of a certain amount of sample heated up to 900 °C for 7 min under an inert flow of Ar. The amount of fixed carbon was determined by difference.

The ultimate analyses of biomass and pyrolysis products (bio-oil, char and coke) were performed in a Thermo Scientific FLASH 2000 CHNS/O micro-elemental analyzer. C, H, N and S elements were directly measured, whilst O was determined by difference. The coke deposited over the catalysts was quantified by TGA. Thereby, a certain amount of the used catalyst was heated up to 550 °C at 20 $°C \cdot min^{-1}$ under air flow and coke was calculated by weight difference. The water content of the bio-oil fraction was measured by means of a Mettler-Toledo V20S compact volumetric Karl-Fischer titrator (ASTM E203-08).

The individual components of the bio-oil fraction were analysed by a Gas Chromatograph coupled to Mass Spectrometer (GC/MS), GC-MS, Bruker® SCION 436-GC, (Electron Energy: 70 eV; Emission: 300 V; He flow rate: 1 $cm^3 \cdot min^{-1}$; Column: WCOT fused silica 30 m x 0.25 mm ID x 0.25 µm). For tentative identification of pyrolysis products, all mass spectra were compared to the NIST EI-MS spectral library (v2.0) with a minimum match score of 700. Due to the high complexity of the bio-oil components, the compounds identified by comparing the mass spectra with the NIST database have been classified according to their main functional groups as follows: carboxylic acids (AC), light oxygenates (LO: aldehydes, alcohols, ketones and ethers), furans (FUR), amines and amides (AMN & AMD), oxygenated aromatics (O-AR), aromatic hydrocarbons (AR) and anhydrosugars (SUG). From the response factors corresponding to a number of compounds representative of those families, it was possible to estimate their concentration in the bio-oil* samples.

The gas fraction was analysed using a dual channel Agilent® CP-4900 Micro Gas Chromatograph (µ-GC), equipped with molecular sieve (Molsieve 5 Å) and HayeSep A columns and a thermal conductivity detector (TCD), using He as carrier gas. The equipment was periodically calibrated with standard gas mixtures of different gas concentrations containing $N_2$ (internal standard), $O_2$, $H_2$, CO, $CO_2$, $CH_4$, $C_2H_4$, $C_2H_6$, $C_3H_6$, $C_3H_8$, $C_4H_8$ and $C_4H_{10}$. Thus, the gas mass yield of the gas fraction and its elemental composition (C, H and O) could be calculated.

The high heating value (HHV) of the gases was determined from those of the individual compounds. The HHV of the biomass, bio-oil, char and coke were calculated from the elemental composition using an empirical correlation [5].

By adding the measured weights of the different products, the total mass balance was closed to the amount of biomass fed with an experimental error lower than 5 wt% in all tests. Details on the procedure used for the mass balance calculations in the catalytic and non-catalytic biomass pyrolysis tests can be found elsewhere [4].

Energy yield associated with a specific pyrolysis product was calculated as the proportion of chemical energy (HHV) retained in this product respecting to that of raw biomass. Likewise, the overall selectivity towards the different deoxygenation products ($H_2O$, CO and $CO_2$) was determined from the relative molar production of these compounds in each test taking into account its oxygen content. The catalytic deoxygenation selectivity was calculated in a similar way but subtracting the contribution of a thermal pyrolysis test to the overall $H_2O$, CO and $CO_2$ production.

**Figure captions**

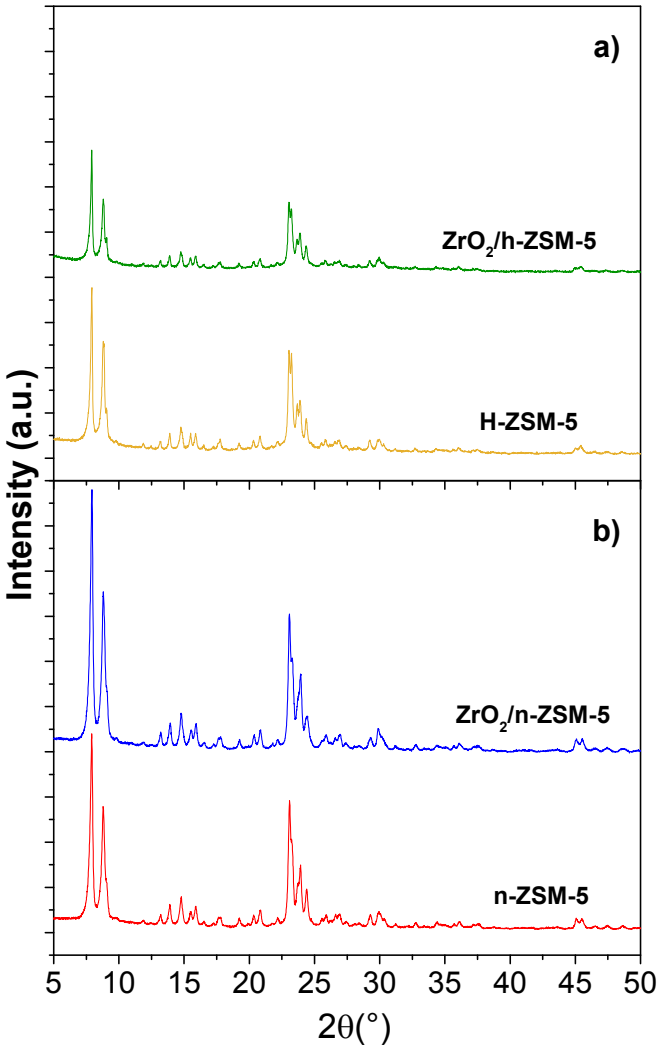


Fig. S1. XRD patterns of calcined (a) desilicated and (b) nanocrystalline ZSM-5 based materials.

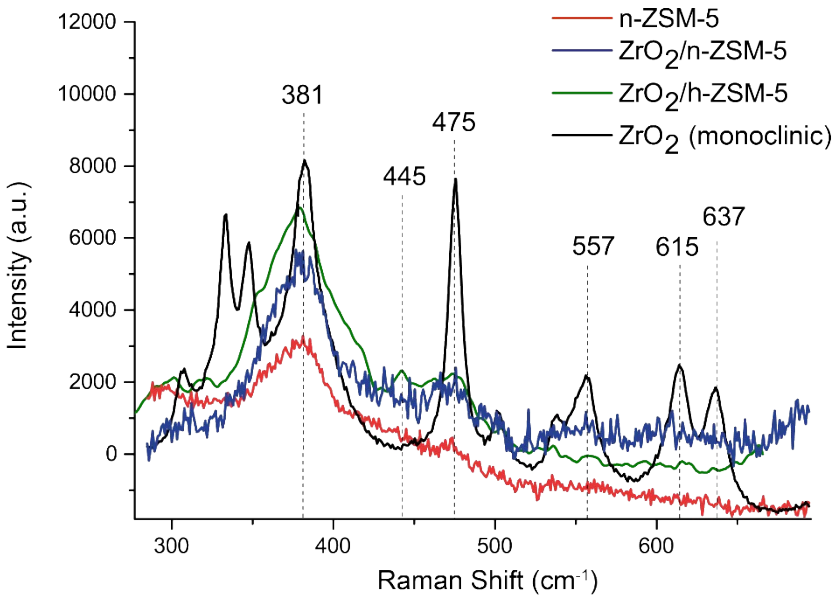


Fig. S2. Raman spectra of n-ZSM-5 (red), $ZrO_2$/n-ZSM-5 (blue), $ZrO_2$/h-ZSM-5 (green) and monoclinic $ZrO_2$ (black), used as reference. Excitation source λ = 785 nm.

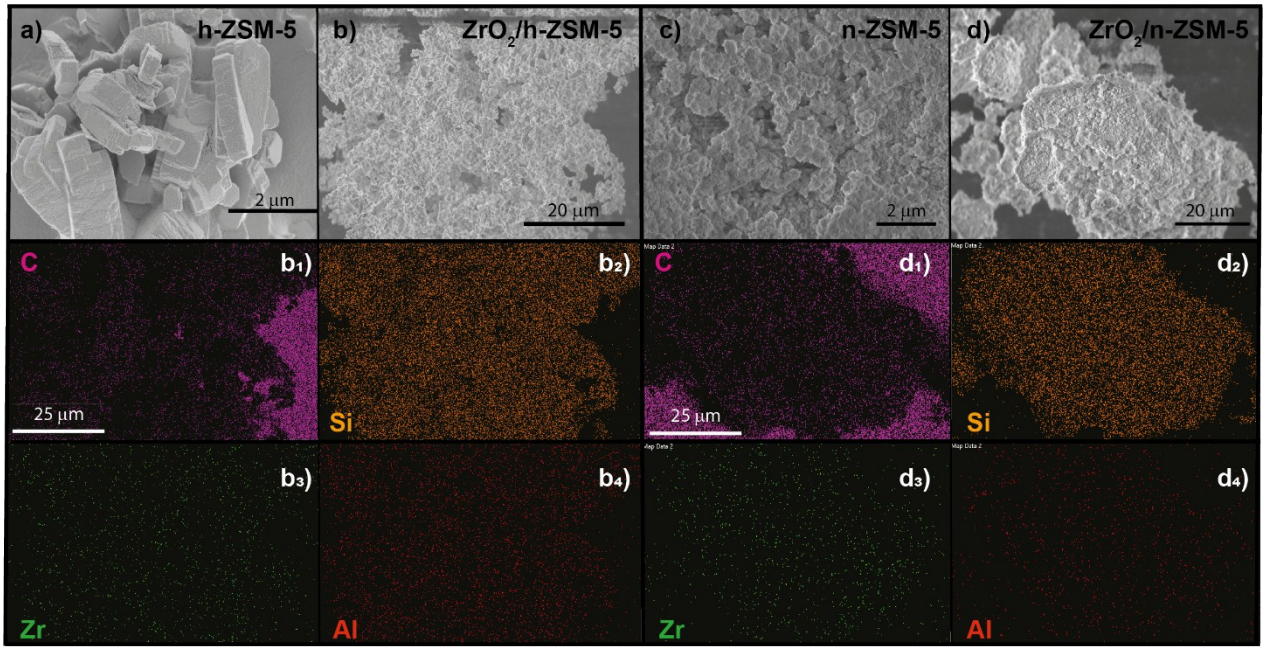


Fig. S3. SEM images of: h-ZSM-5 (a) and n-ZSM-5 (c); and SEM-EDX images and corresponding elementals maps for: $ZrO_2$/h-ZSM-5 (b) and $ZrO_2$/n-ZSM-5 (d) catalysts. Note that dot-mapping of C ($b_1$, $d_1$), present in the carbon sticker which holds the powder sample, is used as reference for defining the negative of the aggregate's contour.

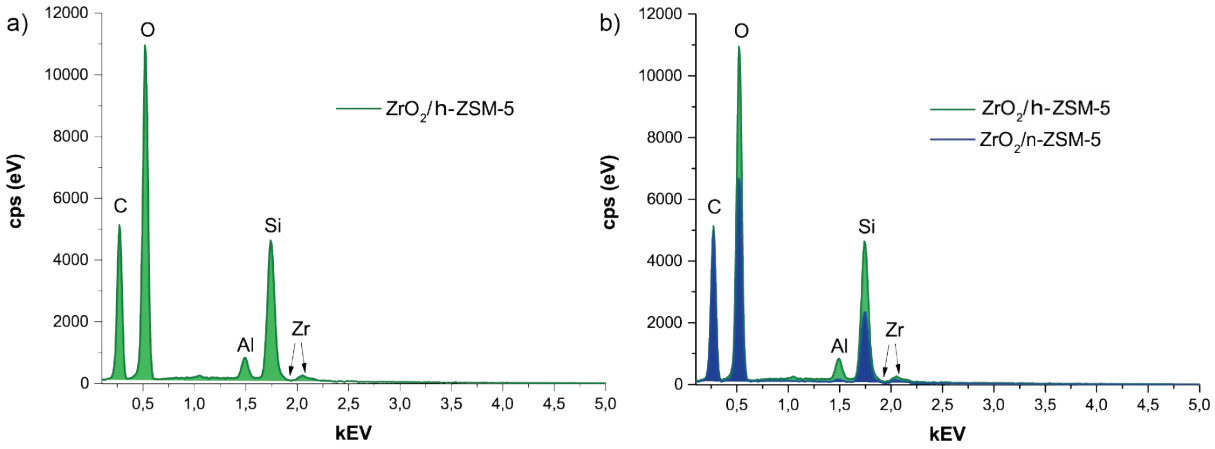


Fig. S4. Map sum spectrum derived from the EDX dot mapping of: a) $ZrO_2$/h-ZSM-5, b) $ZrO_2$/n-ZSM-5 compared to $ZrO_2$/h-ZSM-5.

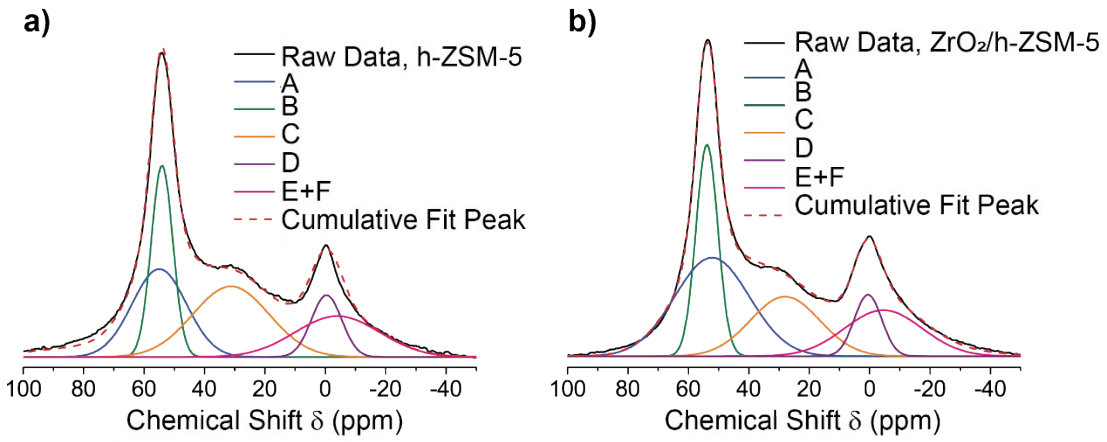


Fig. S5. Deconvolution and fit of the $^{27}$Al MAS ssNMR spectra of h-ZSM-5 (a) and $ZrO_2$/h-ZSM-5 (b).

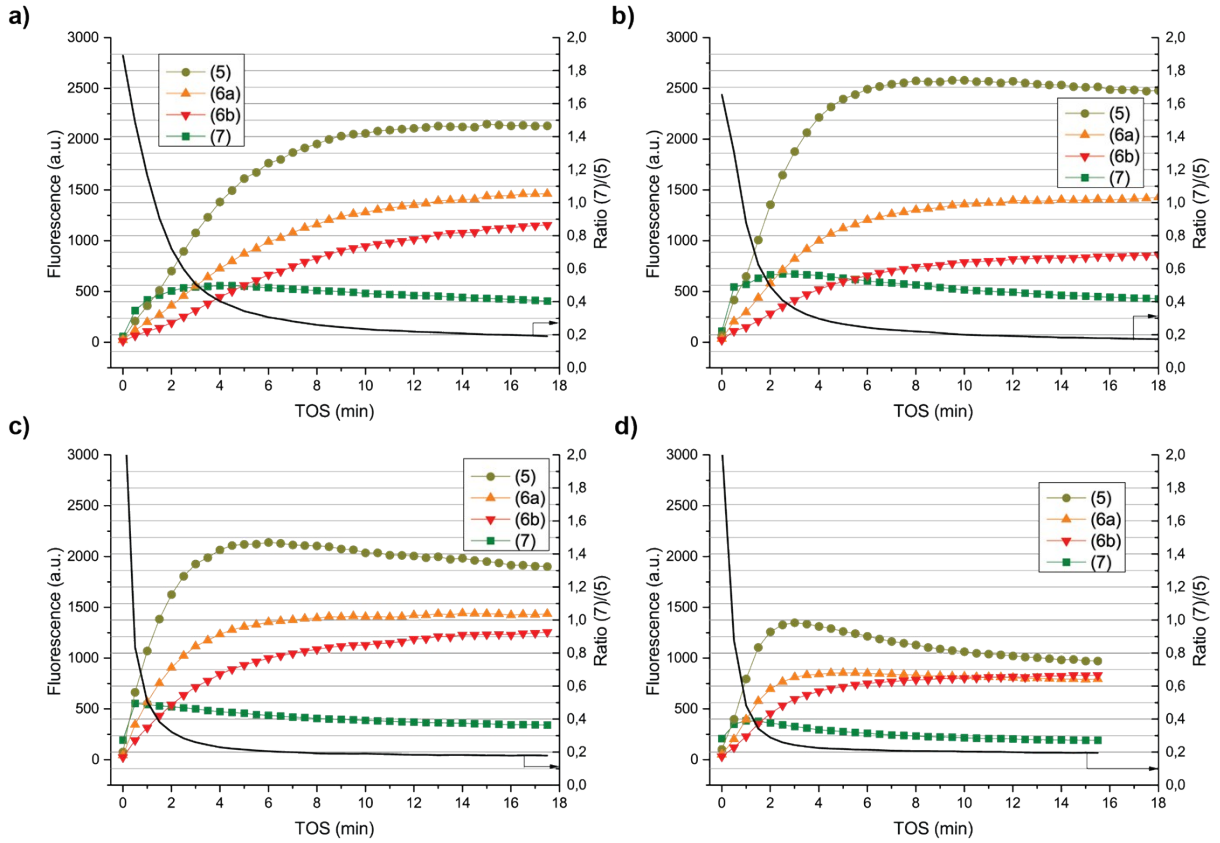


Fig. S6. Left axis: Time evolution of the intensities of the fluorescent emission bands during the 15 min of 4-fluorostyrene oligomerisation at 100 °C on: (a) h-ZSM-5, (b) $ZrO_2$/h-ZSM-5, (c) n-ZSM-5; (d) $ZrO_2$/n-ZSM-5. According to Scheme S1, the corresponding series are assigned to: the cyclic oligomer product (**7**), linear oligomer (**5**), dimer (**6a**) and trimer (**6b**). Excitation lasers: 404, 488, 561, 642 nm. Right axis: Ratio of intensities of the emission bands assigned to cyclic (**7**) and linear (**5**) carbocations at selected times during the 4-fluorostyrene oligomerisation reaction.

Table S1. Resolution of the fitted peaks for the $^{27}$Al MAS ssNMR spectra of h-ZSM-5 and $ZrO_2$/h-ZSM-5 catalysts and ratio of Al species after fitting for both solid catalysts.

| | | **h-ZSM-5** | | **$ZrO_2$/h-ZSM-5** | |
|---|---|---|---|---|---|
| | | Value | Standard Error | Value | Standard Error |
| Peak A | center (ppm) | 54.96 | 0.44 | 53. 84 | 0.99 |
| Peak A | area | 2.79E+06 | 3.24E+04 | 7.93E+06 | 1.02E+06 |
| Peak A | width | 17.96 | 0.75 | 26.50 | 0.62 |
| Peak B | center (ppm) | 54.05 | 0.02 | 52.20 | 0.66 |
| Peak B | area | 2.42E+06 | 5.72E+04 | 5.32E+06 | 47432 |
| Peak B | width | 7.14 | 0.07 | 8.33 | 0.03 |
| Peak C | center (ppm) | 31.24 | 0.48 | 30.56 | 0.75 |
| Peak C | area | 3.16E+06 | 6.52E+05 | 6.09E+06 | 2.33E+06 |
| Peak C | width | 25.27 | 2.37 | 29.64 | 5.48 |
| Peak D | center (ppm) | -0.40 | 0.08 | 1.03 | 0.08 |
| Peak D | area | 1.10E+06 | 7.58E+04 | 1.58E+06 | 174783 |
| Peak D | width | 10.04 | 0.28 | 9.66 | 0.30 |
| Peak E+F | center (ppm) | -3.99 | 2.13 | -3.72 | 1.49 |
| Peak E+F | area | 2.03E+06 | 5.35E+04 | 1.67E+06 | 815078 |
| Peak E+F | width | 28.00 | 2.18 | 18.19 | 2.30 |
| | | **$R^2$ 0.93168** | **Reduced chi-sqr 9.53E8** | **$R^2$ 0.99822** | **Reduced chi-sqr 2.84E7** |

| Sample | $Al^{IV}$ / $Al^{VI}$ | $Al^{IV}$ / $Al^{V}$ | $Al^{IV}/(Al^{VI} + Al^{V})$ |
|---|---|---|---|
| h-ZSM-5 | 3.0 | 3.8 | 1.7 |
| $ZrO_2$/h-ZSM-5 | 2.2 | 2.9 | 1.3 |

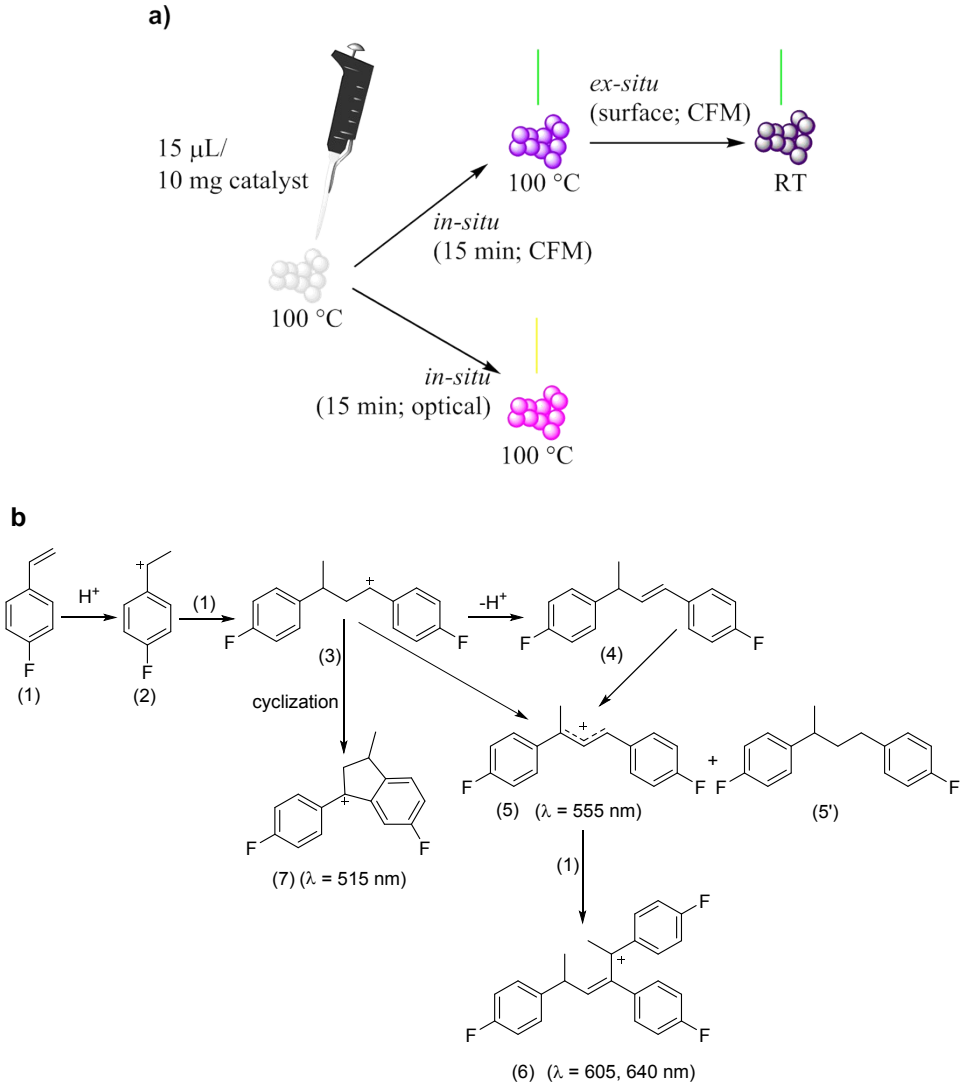


Scheme S1. **a)** Schematic representation of staining of the catalyst under study and in-situ examination by optical microscopy (white light source) and by confocal fluorescence microscopy (CFM) (green to red light source). **b)** Reaction pathways in the Brønsted acid-catalysed oligomerization of 4-fluorostyrene on H-ZSM-5 zeolites [6–8]. 4-fluorostyrene is protonated in the presence of Brønsted acid sites (BAS) giving benzylic carbocation (2). Dimerization with a second 4-fluorostyrene monomer (1) yields the linear dimeric 1,3-bis(4-fluorophenyl)-1-butylium cation (3), which can be transformed either into a conjugated linear dimeric 1,3-bis(4-fluoro- phenyl)-2-buten-1-ylium carbocation (5) by deprotonation, or into 3-methyl-1,4-fluorophenylindanyl by cyclization (7). Conjugate linear dimeric carbocation (5) can further oligomerize trimeric and longer oligomer species (6). The wavelengths in brackets indicate the literature [6] assignment to the carbocationic species shown.

## Notes and references


1 C. A. Emeis, *J. Catal.*, 1993, **141**, 347–354.

2 A. Peral, J. M. Escola, D. P. Serrano, J. Prech, C. Ochoa-Hernandez and J. Cejka, *Catal. Sci. Technol.*, 2016, **6**, 2754–2765.

3 J.-P. Amoreux, C. Fernandez and S. Steuernagel, *J. Magn. Reson.*, 1996, **123**, 116–118.

4 H. Hernando, S. Jiménez-Sánchez, J. Fermoso, P. Pizarro, J. M. Coronado and D. P. Serrano, *Catal. Sci. Technol.*, 2016, **6**, 2829–2843.

5 S. A. Channiwala and P. P. Parikh, *Fuel*, 2002, **81**, 1051–1063.

6 I. L. C. Buurmans, E. A. Pidko, J. M. de Groot, E. Stavitski, R. A. van Santen and B. M. Weckhuysen, *Phys. Chem. Chem. Phys.*, 2010, **12**, 7032–7040.

7 Z. Ristanović, A. V. Kubarev, J. Hofkens, M. B. J. Roeffaers and B. M. Weckhuysen, *J. Am. Chem. Soc.*, 2016, **138**, 13586–13596.

8 L. R. Aramburo, S. Wirick, P. S. Miedema, I. L. C. Buurmans, F. M. F. de Groot and B. M. Weckhuysen, *Phys. Chem. Chem. Phys.*, 2012, **14**, 6967–6973.